BJP BRITISH JOURNAL OF PHARMACOLOGY

BPS BRITISH PHARMACOLOGICAL SOCIETY

British Journal of Pharmacology (2010), 159, 636–649

0007-1188/10
www.brjpharmacol.org

RESEARCH PAPER

Kinetic analysis of evoked IPSCs discloses mechanism of antagonism of synaptic $GABA_A$ receptors by picrotoxin

AR Korshoej, MM Holm, K Jensen and JDC Lambert

Department of Physiology and Biophysics, Aarhus University, Ole Worms Allé 1160, DK 8000 Århus C, Denmark

Background and purpose: Although picrotoxin is a well-established antagonist of $GABA_A$ receptors, detailed studies of its action on inhibitory synaptic transmission have not previously been made.
Experimental approach: Electrophysiological techniques were used to study the action of picrotoxin on inhibitory postsynaptic currents (IPSCs) evoked in hippocampal neurones, in culture and slice preparations prepared from Wistar rat embryos and juveniles, respectively.
Key results: Picrotoxin gradually reduced the amplitude of $GABA_A$ receptor-mediated eIPSCs in a concentration-dependent manner. This was accompanied by a marked acceleration of the eIPSC decay kinetics, which, in contrast to the effect on amplitude, developed immediately and was completely reversed on washing. The decaying phase of the IPSC could be resolved into two components; 30 μM picrotoxin reduced τ_{fast} by 34% and increased its relative amplitude, while τ_{slow} was reduced by 38%, and its relative amplitude decreased. The area under the decaying phase of the normalized eIPSC showed an immediate reduction by 36% in 30 μM picrotoxin. With increasing concentrations of picrotoxin, this normalized area converged towards 55% of the control, indicating that the rate of relaxation and block has a finite maximum. This implies that picrotoxin does not act by a pore-occluding mechanism (open-channel blocking), and suggests allosteric stabilization of desensitized receptor states as a more likely alternative. This was corroborated by modelling, based on two established microscopic $GABA_A$ receptor transition schemes.
Conclusions and implications: Although the identity of the stabilized state has not been determined unequivocally, picrotoxin effectively traps synaptic $GABA_A$ receptors in a desensitized state.
British Journal of Pharmacology (2010) **159,** 636–649; doi:10.1111/j.1476-5381.2009.00542.x; published online 25 January 2010

Keywords: $GABA_A$; IPSC; picrotoxin; cultured hippocampal neurones; allosteric modulation; IPSC decay kinetics; desensitization

Abbreviations: eIPSC, evoked inhibitory postsynaptic current; PTX, picrotoxin

Introduction

Picrotoxin (PTX) is a convulsive compound extracted from plants (Olsen, 2006) and is one of the earliest characterized antagonists of responses to GABA (e.g. Takeuchi and Takeuchi, 1969). Following the first demonstration of specific blockade of GABA receptors by PTX in the central nervous system (CNS) (Curtis *et al.*, 1969), it then played a key role in the initial identification of GABA-mediated inhibition at a variety of sites within the CNS (see review by Curtis and Johnston, 1974). In studies involving complex synaptic interactions, PTX is still employed extensively to block $GABA_A$ receptor-mediated inhibition and thereby provides a means of functional isolation of other receptors and mechanisms for further study.

It has long been recognized that picrotoxin is a non-competitive (Takeuchi and Takeuchi, 1969) or mixed (Smart and Constanti, 1986) antagonist of GABA receptors. Early studies suggested that PTX binds at a site within the channel and thereafter blocks the current through the ionophore (Inoue and Akaike, 1988). Recent findings have brought us closer to identifying the actual binding site. Site-directed mutagenesis identified a polar threonine residue at the 6′ location in the cytoplasmic half of the second transmembrane helix, which, when mutated to a phenylalanine, abolished antagonism by PTX (Sedelnikova *et al.*, 2006). This finding was supported by cysteine scanning mutagenesis, and structural modelling proposes that the pore-lining threonine interacts directly with PTX through hydrogen bonding (Chen *et al.*, 2006). More recently, mutation of the critical 6′

Correspondence: John DC Lambert, Department of Physiology and Biophysics, Aarhus University, Ole Worms Alle 1160, DK 8000 Århus C, Denmark. E-mail: jl@fi.au.dk
Received 4 June 2009; revised 18 August 2009; accepted 22 September 2009

threonine residue led Erkkila *et al.* (2008) to conclude that PTX achieves its greatest efficacy when it makes hydrogen bonds with three adjacent uncharged polar amino acids (on two α- and one μ-TM2 subunits). Moreover, considerations of the relative sizes of the pore and PTX molecule led the authors to suggest that PTX inhibits the channel by a non-competitive pore-blocking mechanism (Erkkila *et al.*, 2008). However, a handful of electrophysiological studies performed on both naturally and artificially expressed $GABA_A$ receptors have led to the proposal that PTX stabilizes a non-conducting (i.e. closed or desensitized) state of the $GABA_A$ ionophore following binding to an allosteric site (Smart and Constanti, 1986; Newland and Cull-Candy, 1992; Dillon *et al.*, 1995; Krishek *et al.*, 1996). Yoon *et al.* (1993) also showed that part of the inhibiting action of PTX on hippocampal neurones results from a conformational change initiated by the binding of GABA to its receptor and therefore has the characteristic of being use dependent. PTX has also been shown to decrease the opening frequency of single $GABA_A$ channels, suggesting stabilization of an agonist-bound, non-conducting state, such as a desensitized conformation (Newland and Cull-Candy, 1992; Porter *et al.*, 1992; Ikeda *et al.*, 1998). More recently, using very rapid (μs) release of GABA from a caged compound onto expressed $\alpha_1\mu_2\gamma_{2L}$ receptors, Ramakrishnan and Hess (2005) have shown that PTX binds with a higher affinity to the allosteric site of the non-conducting channel form than the open-channel form. This resulted in a fourfold reduction of the channel-opening equilibrium constant, thereby stabilizing the closed state.

While the aforementioned studies have been made on patches excised from neurones and expression systems, there appears to be no detailed study of the effects of PTX on inhibitory postsynaptic potentials themselves. Here, we make a detailed analysis of the effect of PTX (3–30 μM) on the kinetics of inhibitory postsynaptic currents (IPSCs) evoked on hippocampal neurones by stimulation of presynaptic GABAergic fibre(s) in both acute slices and culture preparations. Consideration of two established microscopic transition schemes leads us to conclude that PTX blocks $GABA_A$ receptors by allosteric stabilization of desensitized receptor state(s). Part of the work has been presented as abstracts (Holm *et al.*, 2007; Korshoej *et al.*, 2007; Lambert and Korshoej, 2008).

Methods

All procedures were performed in accordance with the guidelines of the University of Aarhus and with the Danish and European Law regarding the use of laboratory animals. Drug and molecular target nomenclature conforms to the British Journal of Pharmacology's Guide to Receptors and Channels (Alexander *et al.*, 2008).

Preparations: cultured neurones

The experiments were performed on dissociated cultured hippocampal neurones (16–22 days *in vitro*) prepared from 19–20-day-old Wistar rat embryos. The pregnant rat was anaesthetized with pentobarbital (50 $mg \cdot kg^{-1}$, i.p.), the foetuses were removed *in utero* and the rat was killed by cutting the major arteries from the heart, in accordance with the guidelines laid down by the Danish Ministry of Justice. The hippocampi were dissected free and mechanically triturated in dissection medium containing (mM) 137 NaCl, 5.4 KCl, 0.3 Na_2HPO_4, 1 $NaHCO_3$, 0.4 KH_2PO_4, 5 HEPES, 30 glucose. pH was adjusted to 7.3 with NaOH. The triturated tissue was plated on poly-D-lysine coated coverslips in 35-mm Petri dishes. Plating medium consisted of minimal essential medium with Earle's salt and Glutamax-1 supplemented with horse serum (HS, 10%) and foetal calf serum (FCS, 10%), penicillin (50 $IU \cdot mL^{-1}$) and streptomycin (50 $\mu g \cdot mL^{-1}$). Cultures were grown in 5% CO_2 at 37°C. Plating medium was replaced completely by 2 mL feeding medium (in which FCS was omitted and HS was reduced to 5%) after 1 day, and, thereafter, 1 mL was exchanged weekly. The mitosis inhibitors, 5'-fluro-2'-deoxyuridine (15 $\mu g \cdot mL^{-1}$) and uridine (35 $\mu g \cdot mL^{-1}$), were added after 3–4 days when cultures showed a confluent background.

Preparations: brain slices

Brain slice experiments were performed on male Wistar rats post-natal day 12–16 (P12–16). Animals were kept in a local university facility and anaesthetized with isoflurane before decapitation. The brain was rapidly isolated from the animal and transferred to an ice-cold artificial cerebrospinal fluid [aCSF (in mM): 126 NaCl, 2.5 KCl, 2 $CaCl_2$, 2 $MgCl_2$, 10 D-glucose, 1.25 NaH_2PO_4 and 26 $NaHCO_3$, osmolality 305–315 mOsm, pH 7.4 when bubbled with 5% CO_2 and 95% O_2]. The brain was glued onto the platform of a Vibratome 3000 Plus (Vibratome Company, St Louis, MO, USA) and completely covered with ice-cold, bubbled aCSF. Coronal slices, 350 μM thick, containing the hippocampus were cut and allowed to rest for 1 h at room temperature in bubbled aCSF; 3 mM kynurenic acid, 0.2 mM ascorbic acid and 0.2 mM pyruvic acid were added to slow down the degradation of the slices. Experiments were performed in the period of 1–4 h after slicing.

Cultured neurones: electrodes and solutions

The coverslip containing the cultured neurones was placed in an electrically isolated stainless steel chamber with a quartz glass bottom and visualized on an inverted Nikon Diaphot 200 differential interference contrast (DIC) microscope (Nikon Corporation, Tokyo, Japan). The chamber was continuously perfused with extracellular solution containing (in mM) 140 NaCl, 3.5 KCl, 1.25 Na_2HPO_4, 10 glucose, 10 HEPES, 2.5 $MgSO_4$, 2.5 $CaCl_2$, 2.6 kynurenic acid (to block all ionotropic glutamate receptors). pH was adjusted to 7.3 with NaOH, and the osmolarity was 310 mOsm.

Patch pipettes were pulled on a Flaming/Brown micropipette puller Model P-97 (Sutter Instruments, Novata, CA, USA) and had resistances of 2–5 MΩ when filled. The presynaptic electrode contained (in mM) 140 KOH, 1 $CaCl_2$, 10 HEPES (free acid), 11 ethylene glycol-bis(β-aminoethyl ether)-N,N,N,N-tetraacetic acid (EGTA), 2 MgATP, 15 NaCl, 2 $MgCl_2$, 0.1 Leupeptin. pH was adjusted to 7.3 with methanesulphonic acid. The osmolarity was adjusted to 290 mOsm with

1 M sucrose or dH_2O. The postsynaptic electrode contained (in mM) 120 CsCl, 10 tetra-ethyl-ammonium-Cl (TEA), 1 $CaCl_2$, 10 HEPES (free acid), 1 $MgSO_4$, 11 EGTA, 4 MgATP, 5 QX-314-Br, 0.1 leupeptin. pH was adjusted to 7.3 with 1 M CsOH, and the osmolarity was 290 mOsm. With the high $[Cl^-]_i$, E_{Cl^-} was ~0 mV, which gave large inward evoked IPSCS (eIPSCs) at the holding potential (V_h) of –70 mV. QX-314 was included to block voltage-gated Na^+ channels, thereby preventing depolarizing GABA responses evoking action potentials in poorly clamped membrane areas. Cs^+ and TEA were also included to decrease the leak conductance of the membrane and thereby increase its length constant.

Postsynaptic series resistance was corrected as much as possible (70–95% at a lag of 10 μs), and neurones were rejected if the series resistance increased to more than 20 MΩ and/or the holding current became greater than –200 pA.

Cultured neurones: dual whole-cell patch-clamp recordings

Dual whole-cell patch-clamp recordings were made from a presynaptic GABAergic neurone and a randomly selected postsynaptic neurone in the vicinity (Jensen *et al*., 1999a; Korshoej and Lambert, 2007).

Neurones were clamped at –70 mV by using Axopatch 200 and 200A amplifiers (Axon Instruments, Foster City, CA, USA), and signals were low-pass filtered at 5 kHz by using an 80 dB/decade Bessel filter. Recordings were sampled and digitized at 10 kHz by using a Digidata 1320A (Axon Instruments). IPSCs were evoked at 0.2 Hz by stepping the presynaptic neurone to 0 mV for 3 ms. This step evoked an action current at the soma, which, after a conduction delay, released GABA-containing vesicles from the terminals. Local application of bicuculline methobromide (10 μM) was used to verify that the eIPSCs were those mediated by $GABA_A$ receptors. The position of the application pipette (tip diameter ~600 μm) was adjusted until maximum reduction of the eIPSC by bicuculline was obtained. Recordings were discarded if eIPSC amplitudes were ≥5% of the control value.

Control eIPSCs were recorded during local application of standard extracellular solution to control for possible effects of perfusion. A solution containing 1, 3, 10 or 30 μM PTX was then perfused for 60 s (wash-in), which is the period occupied by 12 IPSCs evoked at 0.2 Hz. Although insufficient to achieve maximal antagonism of the eIPSCs (cf. Figure 1A), this duration was chosen to ensure that responses during washout were sufficiently large for kinetic analysis. The solution exchange time was assessed by using an open patch electrode placed in the microscope field of view and measuring the change in junction current in response to reducing the ionic strength of the perfusing medium to 10%. The average time elapsed from initiation of solution exchange until >95% of target concentration was reached was ~4 s. One stimulation pulse was therefore omitted following the start of the solution change. Preincubation with PTX before the first IPSC was evoked was therefore ~6 s. The perfusion was then switched back to standard extracellular solution for 60 s (washout). Once PTX had been applied, the chamber was rinsed thoroughly, and a new coverslip was always used for subsequent experiments.

Electrophysiology and data acquisition: brain slices

Whole-cell voltage clamp recordings (Drasbek and Jensen, 2006) were carried out by using a MultiClamp 700B amplifier (Molecular Devices, Sunnyvale, CA, USA). Electrodes were pulled from borosilicate glass (outer diameter = 1.5 mm, inner diameter = 0.8 mm from Garner Glass Company, Claremont, CA, USA) on a DMZ Universal Puller (Zeitz Instruments, Munich, Germany), backfilled with 120 mM CsCl, 3 mM $MgCl_2$, 5 mM EGTA and 10 mM HEPES, pH 7.35 with CsOH, and exhibited resistances of 3–4 MΩ. Cells were clamped at –70 mV, and the temperature in the recording chamber was kept constant at 33–34°C. Data were acquired by using a custom-made LabView-based program (EVAN v. 1.4.2, courtesy of I. Mody, UCLA, CA, USA), low-pass filtered (8-pole Bessel filter) at 3 kHz and digitized at 20 kHz by using a DA converter (BNC-2110, National Instruments, Austin, TX, USA) and a PCI acquisition board (PCI-6014, National Instruments). As a supplementary acquisition program, we used WinWCP v. 3.5.2. (courtesy of Dr John Dempster, University of Strathclyde, Glasgow, UK). We continuously monitored cell capacitance and resistance through the experiment and compensated series resistance by 70%.

Extracellular stimulation

Double-barrelled borosilicate theta-glass stimulation pipettes (OD = 1.5 mm, ID = 1.0 mm, septum = 0.2 mm, from Warner Instruments Inc., Hamden, CT, USA) were pulled and backfilled with aCSF. An electrical field was generated by inserting platinum wires into the theta-glass, enabling us to stimulate presynaptic fibres in the granule cell layer from presumed GABAergic basket cells. After a whole-cell recording had been established in a granule cell, the stimulation electrode was placed in close proximity within the granule cell layer (distance 50–100 μm). Stimulation pulses were generated by a Master 8 stimulator (A.M.P.I., Jerusalem, Israel) and a stimulus isolator A365 (World Precision Instruments, Inc., Sarasota, FL, USA) and applied at 0.2 Hz until an all-or-none eIPSC was detected. The amplitudes of control eIPSCs ranged from 200 to 400 pA. PTX was dissolved in water at 5 mM aliquots and afterwards diluted in aCSF to be applied by bath perfusion (~2 $mL \cdot min^{-1}$). The antagonist reached the slice approximately 3 min after solution switch, and the amplitude of the eIPSCs action gradually decreased within the next 10 min, then achieving a stable equilibrium.

Data analysis: IPSCs in cultured neurones

eIPSCs were analysed with respect to amplitude, 10–90% rise time and various parameters of decay kinetics. Fitting was performed by using PClamp9 software (Axon Instruments). Kinetic parameters of the eIPSC decay were obtained by fitting a multiexponential function, $IPSC(t) = \sum_{i=1}^{n} A_i \exp(-t/\tau_i) + C$, to the decay phase of the normalized eIPSCs using the Chebychev or Levenberg–Marquardt fitting approaches provided by the PClamp9 software package. Normalization prior to kinetic analysis was considered valid, given that the observation that current kinetics was constant and independent of the

reduction in current amplitude during PTX application (see Results). Therefore, responses were considered to arise from different numbers of channels with identical behaviour (see Discussion).

Each trace was inspected visually and rejected if spontaneous IPSCs were present on the decaying phase. Traces were aligned with respect to the peak of the eIPSCs and then averaged within each exposure category (control, wash-in and washout). Because the alignment correlated the current noise at the peak and because the activation process of $GABA_A$ receptors was presumably not complete at the time of peak, fitting was set to start 1 ms after the peak and designated as $t = 0$. To ensure that the eIPSC had returned completely to the baseline, a fitting range of 800 ms was chosen (see Figure 2B). The goodness-of-fit with increasing numbers of exponential terms was evaluated by the correlation of the fit (r^2 value) and by visual inspection of residuals (see Figure 2B,C). In all cases, two terms adequately described the decay of the eIPSC.

The area under the fitted decay curve was also estimated. Although the area does not reveal detailed mechanistic information about the mechanism of action of PTX, it is very sensitive to changes in all kinetic parameters of the decaying phase. Therefore, the area was used to detect and quantify the effects of PTX on the decaying phase. All effects of PTX on decay kinetics were expressed relative to control values.

The kinetics of the activation process were evaluated by means of the 10–90% rise times of the eIPSCs. Although some traces did not display a smooth, rising phase, all traces were included in the analysis.

Data are expressed as mean ± SEM, and statistical significance was evaluated by either paired or two-sample *t*-test, as indicated.

Data analysis: brain slices

Data were analysed in EVAN or WinWCP. eIPSC amplitudes were normalized to the average of the control eIPSCs before PTX was applied. In addition, the response amplitude as a function of time was plotted. We determined the amplitude of the average eIPSC (>10 responses), where PTX had reached an 'inhibiting equilibrium' with the receptors in the synapse, and these normalized values were plotted (see Figure 6). Some eIPSCs were discarded due to contaminating currents from spontaneous events disturbing the peak and decay of the eIPSC.

For the kinetic analysis a double exponential function was fitted to the trace, calculating two τ values and their respective amplitudes. Weighted τ was calculated by using the equation: $\tau_w = A_{fast} \cdot \tau_{fast} + A_{slow} \cdot \tau_{slow}$, where A_{fast} and A_{slow} are the relative amplitudes of each component. Control parameters were calculated based on an average of the responses before PTX was applied to the slice. Kinetics in the presence of 3 μM PTX were estimated for an average response of a series of consecutive eIPSC in a stable equilibrium with 3 μM PTX. For eIPSCs recorded in the presence of 10 and 30 μM PTX, kinetics were analysed from an average of six responses, when the current amplitude was decreased to 30% of the initial response (see Figure 6B–D). We chose this procedure, because 10 and 30 μM PTX at steady state reduced the responses too much (by 75 and 85%, respectively) to yield meaningful analyses of kinetics. Data are expressed as mean ± SEM, with *n* being the number of cells.

Simulation of $GABA_A$ receptor-mediated currents

To facilitate the interpretation of our findings, we performed simulations of $GABA_A$ receptor-mediated currents evoked by a 1 ms application of 1 mM GABA before and following incubation with PTX. The simulation program was written in MATLAB 6 (R12) (Math Works, Natick, MA, USA) and based on solution of the Kolmogorov differential equation (Colquhoun and Hawkes, 1995; Moffatt, 2007), with the initial value condition that all $GABA_A$ receptors are in the unbound native state. The (infinitesimal) transition matrices of the equation were based on two different kinetic schemes of $GABA_A$ receptor transition: a traditional scheme proposed by Jones and Westbrook (1995) (see Figure 7) and a development by Burkat *et al*. (2001) (see Figure 8), which, along with the most relevant states that contribute to macroscopic responses, includes desensitized states in series with the open state. We sought to keep the models as simple as possible (see Discussion) and investigated the interaction of PTX with different receptor states separately, by adding a single non-conducting PTX bound state in series with the receptor state subject to investigation (see Figures 7 and 8). The objective of the simulations was to provide a qualitative assessment of different inhibitory mechanisms. As evident from the Results, effects of PTX on current kinetics saturated (see Figure 3B). Therefore, to simplify the simulations and circumvent assumptions about rate constants of PTX interaction with the receptor, the concentration of PTX was considered to be saturating. At infinitely high [PTX], the added state becomes absorbing, and, thus, the situation can be modelled by setting the 'return' rate constant from the native state of interest to zero. Furthermore, in the case of an open-channel block, the native open state was classified as non-conducting (due to inhibition by PTX).

Allosteric modulation can also be regarded as alterations of the existing rate constants of a model. This notion was adopted in recent work by Bianchi *et al*. (2007), in which a thorough treatment of the predictive relationship between macroscopic current characteristics and allosteric modulation was presented. Therefore, simulations of such mechanisms have not been performed in the present work.

Materials

Glutamax-1 was obtained from Gibco and PTX from Sigma-Aldrich (Brøndby, Copenhagen, Denmark).

Results

Effect of picrotoxin on eIPSCs in cultured neurones: response amplitudes

We investigated the effect of four concentrations of PTX (1, 3, 10 and 30 μM) on the amplitude of IPSCs evoked at 0.2 Hz (Figure 1). PTX was applied for 60 s (equivalent to 12 stimulations) and was followed by a period of washout for 60 s. The amplitude of the first IPSC evoked after the neurones had

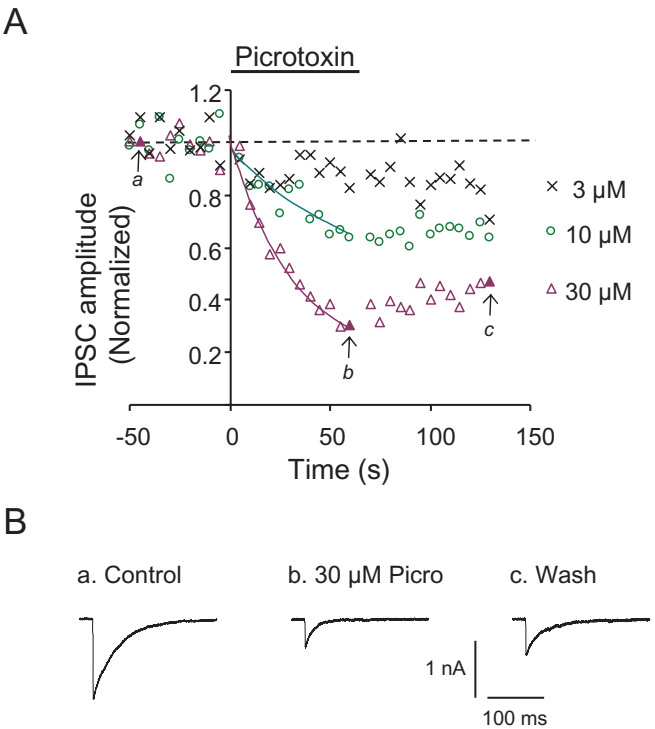

Figure 1 PTX causes a time- and concentration-dependent reduction in the amplitude of $GABA_A$ergic eIPSCs on cultured neurones. Dual whole-cell recordings from a presynaptic GABAergic neurone and a post-synaptic neurone. IPSCs were evoked by stimulation of the presynaptic neurone at 0.2 Hz. (A) eIPSC amplitudes normalized to the average of the control responses in each cell (stippled line) and then averaged (n = 4). PTX was applied by bath perfusion for 60 s (black bar) at the concentrations designated by the symbols. Application of 1 μM PTX did not affect the amplitudes of the eIPSCs, and the data were omitted for clarity. Stimulation was halted at the moment the PTX application was started to ensure that PTX was present when the next stimulation was delivered. The amplitude of the eIPSC was reduced by PTX in both a time- and concentration-dependent manner. Solid lines represent best monoexponential fit to the data for 10 and 30 μM within the application period (see text). For both concentrations, the block reverses slowly and incompletely within a period of 60-s washing. (B) Averages of four eIPSCs identified by solid symbols in (A). These were recorded (a) before, (b) 60 s after start of perfusion with 30 μM PTX and (c) 60 s after washing. PTX caused a decrease in amplitude to 31% that only reversed to 47% of the initial size following washing. Further kinetic analysis of these results is presented in Figure 2. PTX, picrotoxin.

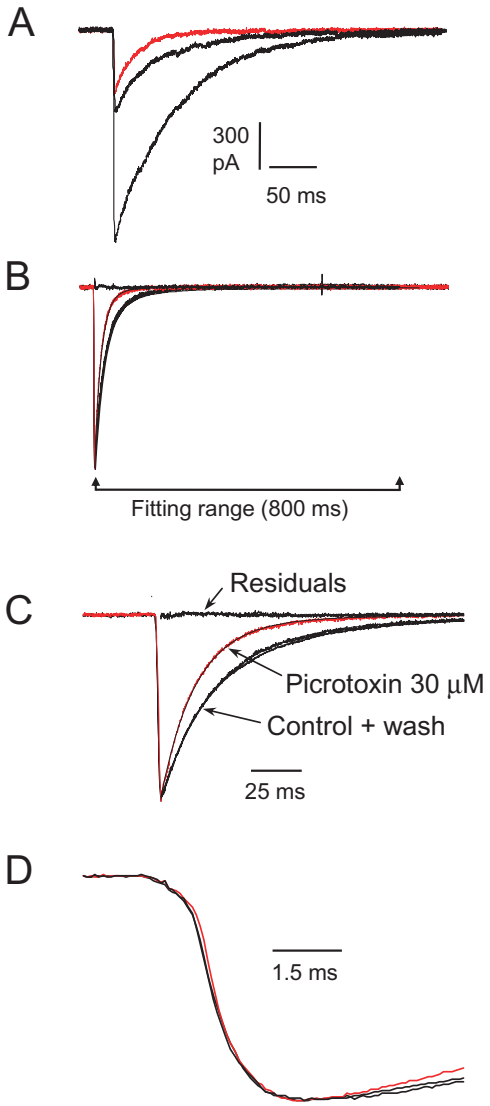

Figure 2 PTX causes a readily reversible change in the recovery kinetics of the eIPSC on cultured neurones. (A) Superimposed averages of the same eIPSCs shown in Figure 1B (n = 4) recorded before (black trace (Figure 1Ba), 1574 ± 193 pA), 60 s after start of perfusion with 30 μM PTX (red trace (Figure 1Bb), 453 ± 61.5 pA) and 60 s after washing (black trace (Figure 1Bc), 551 ± 117 pA). (B) Same averaged eIPSCs as in (A) normalized to the same peak and superimposed. The bar below the traces represents the fitting range, which started 1 ms after the peak and finished after 800 ms, when all traces had returned completely to base line. The thin line (which is mainly obscured by the traces of the eIPSCs) shows the regression line of the best double exponential fit to the data (see text). PTX caused an acceleration of the decay kinetics (red trace), and this effect was completely reversible on washing. (C) Same traces as in (B), but on a five times faster time scale to emphasize the change in kinetics. The residuals about the regression line are displayed on the baseline and represent the goodness of the fit. Control and wash-out traces can only just be distinguished from each other. (D) Same traces as in (A) and (B) on an even faster time scale to demonstrate that the rising phase is little affected by PTX. Note that acceleration of the decay phase in the presence of PTX starts just after the peak.

been exposed to PTX for 6 s was not altered with respect to the control (for 30 μM PTX: two-sided P = 0.24, two sample t-test). Otherwise, the application of PTX resulted in a time- and concentration-dependent reduction of eIPSCs amplitudes (Figure 1A). PTX 1 μM had no significant effect on the eIPSCs after 60 s (not shown), while 3 μM reduced the amplitude by 19 ± 9.2%. PTX 10 and 30 μM reduced the eIPSC by 36 ± 8.0% and 69 ± 5.9%, respectively. The decrease in amplitude halted abruptly at the onset of washing. However, there was little recovery, as evaluated by the difference between the last response recorded during PTX application and after 60 s of washing. Recovery was by 0.0 ± 8.8% for 10 μM PTX and 16 ± 11% for 30 μM PTX (Figure 1A). The amplitude decrements during exposure to 10 and 30 μM PTX were fitted by a monoexponential expression of the form, $A{\cdot}exp(-t/\tau) + C$ (solid lines in Figure 1A). C is the proportion of the response remaining after long exposures to PTX. For 10 μM PTX, A was 0.51 ± 0.27, τ was 60 ± 54 s and C was 0.46 ± 0.29. For 30 μM, the values were 0.85 ± 0.063, 31 ± 5.8 s and 0.18 ± 0.071, respectively.

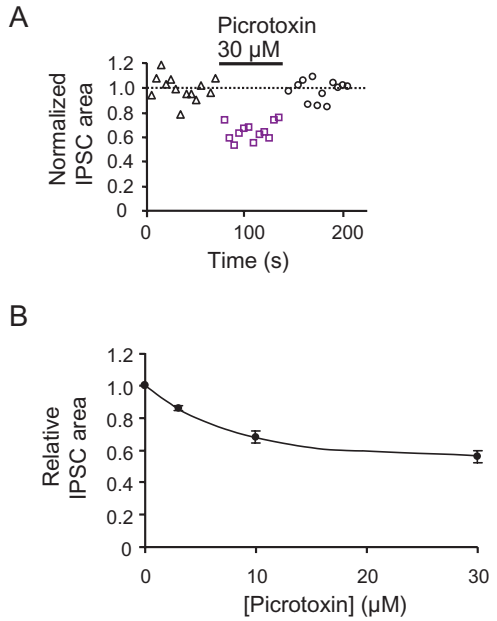

Figure 3 PTX caused a rapid and reversible reduction in the relative area of the eIPSC on cultured neurones. (A) The average relative areas under the normalized eIPSCs (n = 4, error bars omitted for clarity). IPSCs were evoked at 0.2 Hz. Estimates were normalized to the average of control responses within the same cell before calculating the average (paired effect) between cells. For 60 s (black bar), 30 μM PTX was applied. The normalized area of the eIPSCs showed an immediate reduction by 35 ± 2.1% (squares), which was immediately reversible on washing (circles). (B) Plot of the average relative area under the normalized eIPSCs as a function of PTX concentration (μM). Area estimates were normalized to the average area of the control responses within the same cell. These estimates were then averaged (n = 6–12) within the PTX application period to evaluate the paired effect of PTX in each cell. This approach was considered valid given the rapid and stable effect of PTX within the application period (A). These estimates were then averaged and plotted for 3, 10 and 30 μM PTX (±SEM; n = 4). The solid line represents the best monoexponential fit to the data (see text). The curve converges towards a value for the normalized area of 0.55 ± 0.035, which indicates a finite maximum rate of relaxation and block (see text).

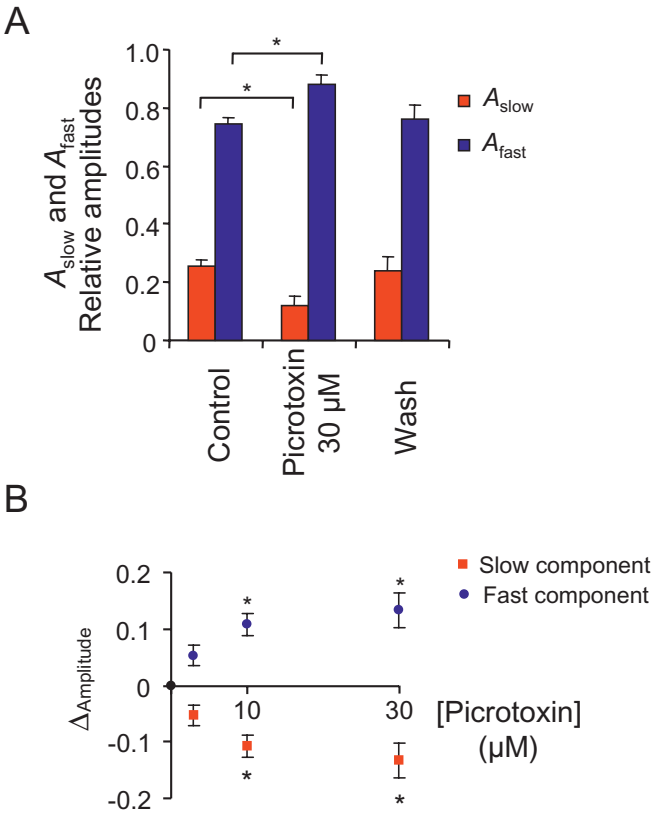

Figure 4 PTX alters the relative amplitudes of fast and slow components of the eIPSC decay on cultured neurones. (A) Average of the relative amplitudes (±SEM, n = 4) of the two exponential fitting terms used to describe the fast and slow components the eIPSC decay. Note that these add up to 1.0 in each case. PTX 30 μM significantly increases the relative amplitude of the fast component by 13% (P < 0.05), with a corresponding reduction in the relative amplitude of the slow component. The effect of PTX was completely reversed upon wash out. (B) Concentration-dependence of the effect of PTX ($\Delta_{Amplitude}$) on the relative amplitudes of the slow and fast components. At concentrations of 3, 10 and 30 μM (n = 4), PTX caused a concentration-dependent increase in the relative amplitude of the fast component (and corresponding decrease in the relative amplitude of the slow component) (P > 0.05 at 3 μM and <0.05 at 10 and 30 μM (*)).

Effect of picrotoxin on eIPSCs in cultured neurones: response kinetics

Figure 2 shows the effect of 30 μM PTX on the kinetics of the same eIPSCs shown in Figure 1B. On normalization of all responses, it is apparent that PTX causes a marked and completely reversible acceleration of the decay phase of the eIPSC (Figure 2B,C). Furthermore, these effects on all kinetics parameters were constant and independent of the eIPSC amplitude during the application of PTX. Therefore, it was considered valid to base further kinetic analysis on normalized currents because they were all assumed to arise from different numbers of channels with identical behaviour (see Methods and Discussion). PTX had no significant effect on the rising phase (Figure 2D). The absolute estimate of the 10–90% rise times of control eIPSCs was 1.69 ± 0.15 ms, which was not significantly different from that in the presence of PTX (1.66 ± 0.23 ms at 30 μM PTX; paired t-test gave two-sided P > 0.8 at all concentrations of PTX).

Effect of picrotoxin on eIPSCs in cultured neurones: area

As mentioned in Methods, the area under the normalized eIPSCs is a particularly sensitive indicator of changes in the decaying phase. This area was reduced by 35 ± 2.1% during application of 30 μM PTX (Figure 3A). The reduction occurred promptly and was constant throughout PTX application. Recovery was rapid and complete upon washout. Furthermore, the reduction by PTX was concentration dependent, as shown in Figure 3B.

Without prior knowledge of the nature of the interaction between PTX and the $GABA_A$ receptor, it was not possible to derive a precise expression to describe the relationship between normalized area and PTX concentration. However, given the stochastic nature of channel behaviour, exponential component(s) are likely to appear in such an expression. A monoexponential model was therefore chosen:

$$NA([PTX]) = \frac{Area([PTX])}{Area([PTX]=0)} = (1 - NA([PTX]=\infty)) \cdot \exp\left(\frac{-[PTX]}{\alpha}\right) + NA([PTX]=\infty), \quad (1)$$

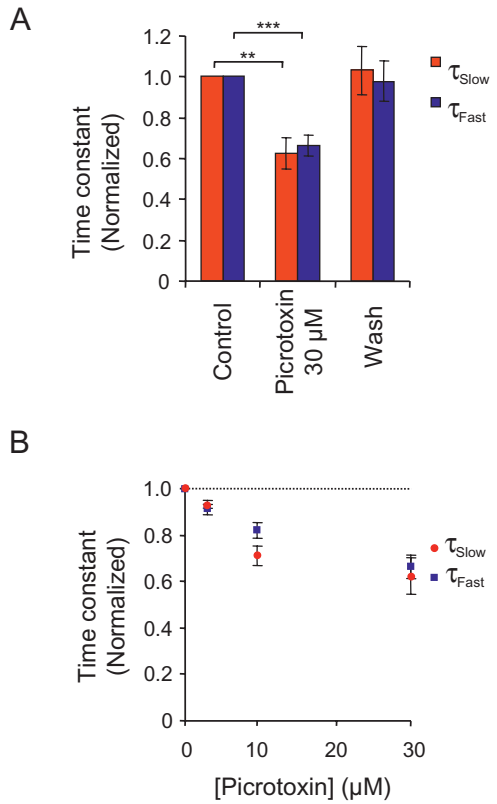

Figure 5 Concentration-dependence of the effect of PTX on the eIPSC decay time constants on cultured neurones. (A) The control slow and fast decay time constants have been normalized to 1.0. Paired results from four neurones. 30 μM PTX reduced both the slow- and fast-time constants to a similar extent (by 38% ($P < 0.05$) and 34% ($P < 0.01$), respectively), and the effect was completely reversed on washing. (B) Normalized time constants as a function of the applied concentration of PTX. PTX caused a concentration-dependent reduction of both time constants by similar proportions (see text for further details).

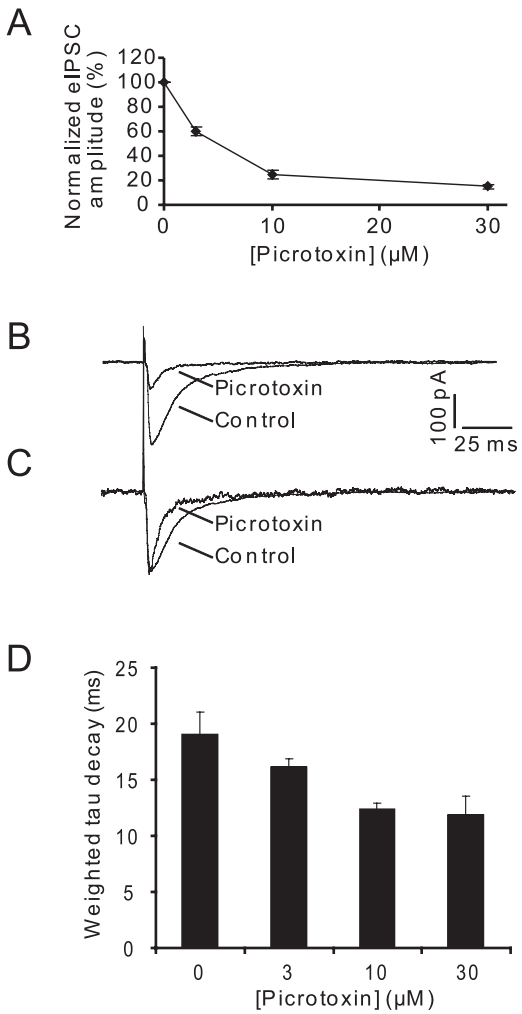

Figure 6 PTX reduced the amplitude and accelerated the decay of eIPSCs in brain slices. The experiments were performed in freshly prepared brain slices by using extracellular stimulation. For each experiment, one concentration of PTX was applied by changing the perfusion buffer. We stimulated at 0.2 Hz, and the evoked IPSCs gradually decreased until a plateau amplitude was reached. This level was normalized to the amplitude of the initial control amplitude and plotted in (A). (B) Average traces recorded before ('control') and after ('picrotoxin') 30 μM PTX was applied to the slice. In (B) through to (D), 10 and 30 μM was analysed when their amplitudes were depressed to 30% of the initial value (see Methods). (C) Same responses as in (B), except that amplitudes have been normalized. In this experiment, the average weighted τ decay changed by 40% during the application of PTX (from 18 to 9.8 ms). The small, transient current observed immediately before the rising phase represents a partially blanked stimulation artefact, caused by the stimulating electrode. (D) Decay kinetics of responses inhibited by different PTX concentrations.

where $NA([PTX])$ represents the area of the normalized eIPSC at a given PTX concentration, [PTX], relative to the control eIPSC area, and α is the 'concentration constant' (i.e. reciprocal rate constant) of normalized amplitude decay. The estimated value of the fitting parameters is $NA([PTX] = \infty) = 0.55 \pm 0.035$ [and is significantly larger than zero (two-sided $P < 0.0001$)], while $\alpha = 7.89 \pm 2.22\ \mu M^{-1}$.

Certain qualitative features can be deduced from the analysis. $NA([PTX] = \infty)$ is a particularly interesting parameter because it indicates that approximately 55% of the normalized eIPSC area is still present at a high concentration of PTX. In other words, the effects of PTX on current kinetics saturates at high concentrations (see Discussion).

Effect of picrotoxin on eIPSCs in cultured neurones: time course of decay

Paired changes in each exponential fitting parameter following the application of PTX were estimated by normalization to the average value for all control eIPSCs ($n = 12$). Decay phases of these control responses were characterized by two exponential terms, one of which had a relatively small time constant ($\tau_{fast} = 33 \pm 1.8$ ms) and large relative amplitude ($A_{fast} = 0.70 \pm 0.015$), while the other had a relatively large time constant ($\tau_{slow} = 102 \pm 8.1$ ms) and small relative amplitude ($A_{slow} = 0.30 \pm 0.015$).

Application of higher concentrations of PTX (>3 μM) caused an immediate shift in the relative amplitudes of the two components, with a reduction in A_{slow} and a corresponding increase in A_{fast} (two-sided $P > 0.05$ at 3 μM and $P < 0.05$ at 10 and 30 μM, paired *t*-test). We examined the absolute amplitudes to disclose what lay behind this change in the relative contributions. While both components were reduced

by PTX, the slow component was reduced to a greater extent than the fast component (data not shown). The effect appeared to saturate and was immediately and entirely reversible upon washout (Figure 4).

Apart from the effects on relative amplitudes, the absolute values of both τ_{fast} and τ_{slow} were reduced upon the application of PTX. For 30 μM PTX, τ_{fast} decreased from 31 to 20 ms (two-sided $P < 0.05$, paired *t*-test), while τ_{slow} decreased from 98 to 59 ms ($P < 0.01$), which is a reduction of similar proportions (τ_{fast} by 33.5% and τ_{slow} by 37.5%; Figure 5A). This reduction of both time-constants occurred immediately upon the application of PTX and was readily and completely reversible upon washout, as was the case for all other kinetic parameters.

Effects of picrotoxin on eIPSCs in brain slices: response amplitudes and kinetics

To confirm that the acceleration of the IPSC decay by PTX could also be observed in intact brain tissues, we employed extracellular stimulation in the dentate gyrus to activate GABAergic synapses on granule cells. By using a thin theta-glass, axonal fibres projecting from a presumed GABAergic basket cell were stimulated. By recording from the target granule cell, we analysed the waveform of the eIPSC during bath perfusion of different concentrations of PTX (3, 10 or 30 μM).

Upon perfusion, PTX gradually reduced the amplitude of the eIPSC. Each experiment was completed after the amplitude of the eIPSCs had reached a plateau during the application of one concentration of PTX. By using different PTX concentrations, the normalized plateau amplitude is plotted in Figure 6A. Perfusion of 3 μM PTX progressively resulted in responses with amplitudes at 60 ± 4.0% ($n = 3$); 10 μM reduced the eIPSCs to 25 ± 3.4% ($n = 4$), while 30 μM PTX antagonized responses to 15 ± 1.4% ($n = 5$) of the control amplitudes. At the end of most experiments, bicuculline (>60 μM) was added, which completely blocked the residual currents, confirming that the evoked responses were mediated by synaptic transmission and probably via $GABA_A$ receptors (Li and Slaughter, 2007).

Current kinetics were accelerated concurrently with the reduction in response amplitude (Figure 6B–D). A double-exponential expression was fitted to the average traces, and a weighted tau value was calculated, based on a slow and fast component. For control responses with no PTX added, τ_{fast} was 11 ± 1.2 ms, and τ_{slow} was 53 ± 6.4 ms, corresponding to a weighted τ of 19 ± 1.8 ms ($n = 10$). The relative amplitudes were A_{fast} = 76 ± 3.5% and A_{slow} = 24 ± 3.5%, respectively. 3 μM PTX accelerated the decay to a τ_w of 16 ± 0.78 ms (τ_{fast} = 8.19 ± 1.45 ms and τ_{slow} = 32.63 ± 0.78 ms; $n = 3$); 10 μM PTX resulted in τ_w at 12 ± 0.51 ms (τ_{fast} = 7.5 ± 0.73 ms and τ_{slow} = 53.2 ± 9.59 ms; $n = 3$), while 30 μM PTX resulted in τ_w = 12 ± 1.6 ms (τ_{fast} = 6.87 ± 0.77 ms and τ_{slow} = 37.83 ± 2.08 ms; $n = 4$, Figure 6B–D).

Detailed kinetic analysis in slices was complicated by the following factors: (i) individual evoked IPSCs had small amplitudes that were depressed further by PTX; (ii) contaminating spontaneous synaptic activity made it difficult to estimate the kinetic parameter; and (iii) the slow rate of solution exchange often precluded the study of eIPSCs after washout of PTX.

However, the results in brain slices confirm that PTX also accelerates the IPSC decay and reduces IPSC amplitudes in intact brain tissues. This corroborates the results obtained from culture preparations and indicates that these findings are not artefacts of the culturing approach.

Discussion

The site of action of picrotoxin

PTX is an equimolar mixture of picrotin and picrotoxinin, and the latter is active at $GABA_A$ receptors (Olsen, 2006). Both constituents can have actions at other receptors, such as glycine receptors (Wang *et al.*, 2007). PTX can also block nicotinic cholinoceptors (Erkkila *et al.*, 2004) although the IC_{50} is at least an order of magnitude greater than that shown for PTX in the present study. Nevertheless, the fact that 10 μM bicuculline abolished the IPSCs makes us confident that we have indeed been studying the effect of PTX on $GABA_A$ receptors. Blocking presynaptic $GABA_A$ autoreceptors could, in theory, reduce GABA release from the presynaptic terminals and reduce the size of the IPSC. However, this is considered unlikely because presynaptic $GABA_B$ autoreceptors on the relatively exposed terminals are not activated to any appreciable extent by spillover of synaptically released GABA (Jensen *et al.*, 1999b).

Effect of picrotoxin on eIPSC amplitudes

The experiments show that PTX markedly reduces the amplitudes of eIPSCs in a concentration-dependent manner. This reduction is gradual and reverses extremely slowly upon washout (Figure 1). These findings corroborate those of other studies (Yoon *et al.*, 1993; Dillon *et al.*, 1995) and indicate a high affinity of PTX for its site of action on the blocked or non-conducting $GABA_A$ receptor and that this affinity is partly governed by a very slow dissociation rate constant.

It has previously been shown in a variety of tissues that preincubation with PTX alone can induce a block but that the rate of block is facilitated by concomitant exposure to GABA (Newland and Cull-Candy, 1992; Yoon *et al.*, 1993; Dillon *et al.*, 1995). Moreover, GABA has been shown to increase the rate of recovery from the block by PTX (Newland and Cull-Candy, 1992; Yoon *et al.*, 1993). PTX has thus been characterized as both a time- and use-dependent antagonist. Taken together, these results indicate that binding by GABA to its receptor exposes the PTX binding site and thereby facilitates both binding and unbinding of the antagonist (Newland and Cull-Candy, 1992). While these earlier findings would be consistant with the presently demonstrated reduction of eIPSC amplitude on hippocampal neurones, it is presently not possible to distinguish unequivocally between time- and use-dependent components of the block on the basis of amplitude reduction alone (see Future Perspectives). However, the fact that the eIPSC amplitude is initially unchanged after exposure to PTX (Figure 1A) suggests that an immediate reduction of the peak open probability of the $GABA_A$ receptors does not contribute significantly to the inhibition. Rather, the

exponential character of the following decline in amplitude (Figure 1A) is in accordance with a proportional decline of the number of channels available to be activated by subsequent GABA release. This is also supported by poor reversibility on washing (Figure 1A), which indicates very slow dissociation of PTX from its receptor. Thus, once blocked by PTX, receptors are essentially unable to participate in subsequent IPSCs. Kinetic arguments presented below provide further support for this hypothesis and suggest virtually irreversible accumulation of receptors in PTX-bound desensitized states as a common explanation for the effects of PTX on both eIPSC amplitude and kinetics. Furthermore, because use-dependent mechanisms are reflected in the effects of PTX on current kinetics, we have focused on this issue throughout the remaining discussion. For likely mechanisms of inhibition to be approached, eIPSCs were simulated in the limiting case of infinite PTX concentration (see below and Methods).

Effect of picrotoxin on current kinetics

The consistent, abrupt and reversible change in kinetics *during* exposure to PTX (Figures 2 and 3) must represent the actual entry into PTX-bound, non-conducting states. These receptor complexes are essentially excluded from further participation in IPSCs and PTX effectively eliminates a constant proportion of the activated channel population following each synaptic release of GABA. This notion is supported further by two observations: (i) in the presence of PTX, IPSC kinetics were constant and independent of the peak amplitude, indicating that IPSCs were generated by progressively fewer channels with identical behaviour; and (ii) the kinetics of normalized control eIPSCs and those following washout were indistinguishable at all concentrations of PTX (Figure 2, only 30 μM shown). This indicates that responses after washout of PTX were generated by the same processes as control responses, namely, native receptors that had not interacted with PTX during the exposure, while those that still bind PTX remain inactive.

While the marked acceleration of decay kinetics (Figure 2) is consistent with use-dependent processes, it is important to emphasize that there is a finite upper limit on the rate of current decay in the presence of even high concentrations of PTX (55%, Figure 3B). Therefore, some of the available (i.e. unblocked) receptors must be activated before being blocked use-dependently by PTX during the synaptic release of GABA. This observation constitutes the main conclusion of the present study, and allows us to address important issues regarding the mechanism of block by PTX. In the following, we discuss if and how an open-channel block and/or allosteric modulation, such as stabilization of non-conducting (e.g. desensitized) states, can be reconciled with the finite rate of decay. As will be evident below, the observation of a finite rate of decay, together with the analyses of simulated eIPSCs and comparison with single channel studies, provides the ground for dismissing an open-channel block as a likely mechanism of inhibition and emphasizes stabilization of desensitized states as the most likely explanation. Prerequisites for this discussion are as follows: (i) IPSCs are mediated by one specific subtype of $GABA_A$ receptor that has identical pharmacokinetic properties. Mangan *et al.* (2005) have shown that α1, α2, β2/3, γ2 subunits are clustered together on cultured hippocampal neurones and co-localize with GAD65 and are therefore thought to represent the synaptic receptors. (ii) The native transition schemes (see Methods) have been supplemented by PTX-bound receptor states (see Figures 7 and 8). (iii) The concentration of PTX is assumed to be uniform at all membrane areas that contribute to the response, as was confirmed by local application of bicuculline (see Methods).

The case for open-channel block by PTX

As mentioned in the Introduction, PTX has previously been proposed to act, at least in part, as an open-channel blocker. Erkkila *et al*. (2008) reasoned that the $GABA_A$ channel pore, which is 7.2 Å at its narrowest point, would be effectively eclipsed by the PTX molecule (major diameter of about 5.4 Å),

Figure 7 Simulation of the interaction of PTX with the $GABA_A$ receptor based on the kinetic scheme proposed by Jones and Westbrook (1995). (A) Kinetic scheme showing transitions presented by Jones and Westbrook (1995) for the native $GABA_A$ receptor (states shown in black), using their rate constants, as shown. The $GABA_A$ receptor can bind two molecules of GABA (G) to give $Bound_1$ and $Bound_2$, respectively. Each of these can undergo conformational changes to give open, conducting (O_1, O_2) or desensitized (D_1, D_2) states. For all of the conformations, extra states are indicated (in red) that could potentially arise by binding of PTX (P). With an infinitely high concentration of PTX, the return rate constant in each case is effectively zero. By the same token, it is not necessary to consider rate constants for entry into PTX-bound states (see *Methods*). (B) Simulation of occlusion of O_1 (blue) and O_2 (red). (C) Stabilization of $Bound_2$ (cyan), D_1 (green) and D_2 (magenta) responses, respectively. Control simulations are shown in black. (Note that traces showing a great degree of overlapping have been revealed for clarity by displacing very slightly on the ordinate.) In (B) and (C): (a) the open probability of the simulated responses; (b) responses normalized to peak amplitude and expressed on a negative scale to correlate with the recorded IPSCs (*cf.* Figure 2B and D, respectively); (c) same as (b), but on a faster time scale to emphasize the rising phases and early decay kinetics; (d) responses evoked by single stimuli. Peak amplitudes are normalized to control values. A supramaximal concentration of PTX was added at the time of the third stimulus. Occlusion of O_2 has no immediate effect on the peak open probability (amplitude of the first response after exposure to PTX) or the kinetics (Ba–c). However, with repeated stimulation, the amplitude declined slowly (Bd). Occlusion of O_2 results in a marked reduction of peak open probability of the initial PTX response (Ba), which accounts for the abrupt reduction in amplitude upon initialization of repeated stimulation (Bd). Furthermore, normalized responses show marked acceleration of decay kinetics (Bb,c), as well as a more rapid rate-of-rise and shorter time-to-peak (Bc). Thus, both O_1 and O_2 occlusion demonstrate notable dissimilarity with the experimental observations and are considered unlikely mechanisms. Stabilization of $Bound_2$ results in a marked reduction of the initial peak open probability (Ca) and abrupt reduction in the amplitude with repeated stimulation (Cd). Furthermore, normalized responses display a more rapid rate-of-rise, shorter time-to-peak and acceleration of decay kinetics (Cb,c). Stabilization of D_1 is virtually indistinguishable from the control (Ca–c) and demonstrates a gradual reduction in peak amplitude (Cd). Stabilization of D_2 does not affect the initial peak open probability (Ca) and rise-time (Cc), while the decay is accelerated (Cb,c), and there is a gradual reduction in amplitude upon repeated stimulation (Cd). While stabilization of $Bound_1$ and D_1 are not in accordance with the experimental findings, stabilization of D_2 shows close qualitative similarity and is thus a very likely mechanism of PTX inhibition.

and thereby occlude Cl^- ions [diameter of about 3.6 Å, (Halm, 1998)]. Indeed, this notion supports the fact that a pore-lining threonine residue in the $GABA_A$ receptor is crucial for the association of PTX with its receptor (Sedelnikova *et al.*, 2006). A pore-blocking mechanism would also be in accordance with a reduction of intraburst open duration in the presence of PTX. Although a modest reduction of this kind was reported by Twyman *et al.* (1989), an allosteric mechanism was nevertheless proposed as the most likely explanation for the observation (Twyman *et al.*, 1989). Furthermore, the channel blocking hypothesis did not find support in other single channel studies, which failed to show a reduction of mean open time (Newland and Cull-Candy, 1992; Ikeda *et al.*, 1998).

In the case of an open-channel block, at least one open state must exist to which PTX has access and can block. It follows from the law of mass action that PTX at very high concentrations will occlude any PTX-sensitive open state before passage

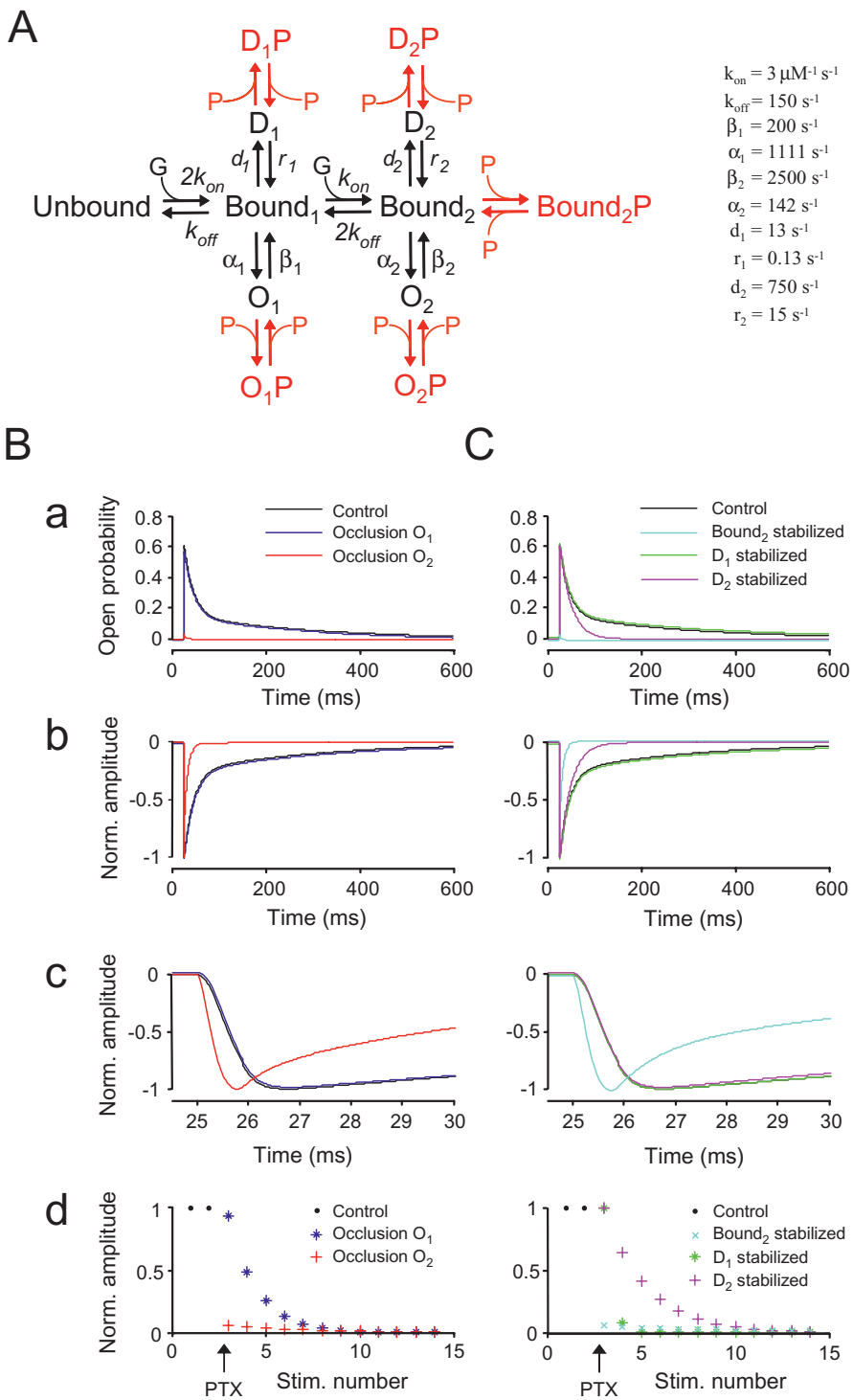

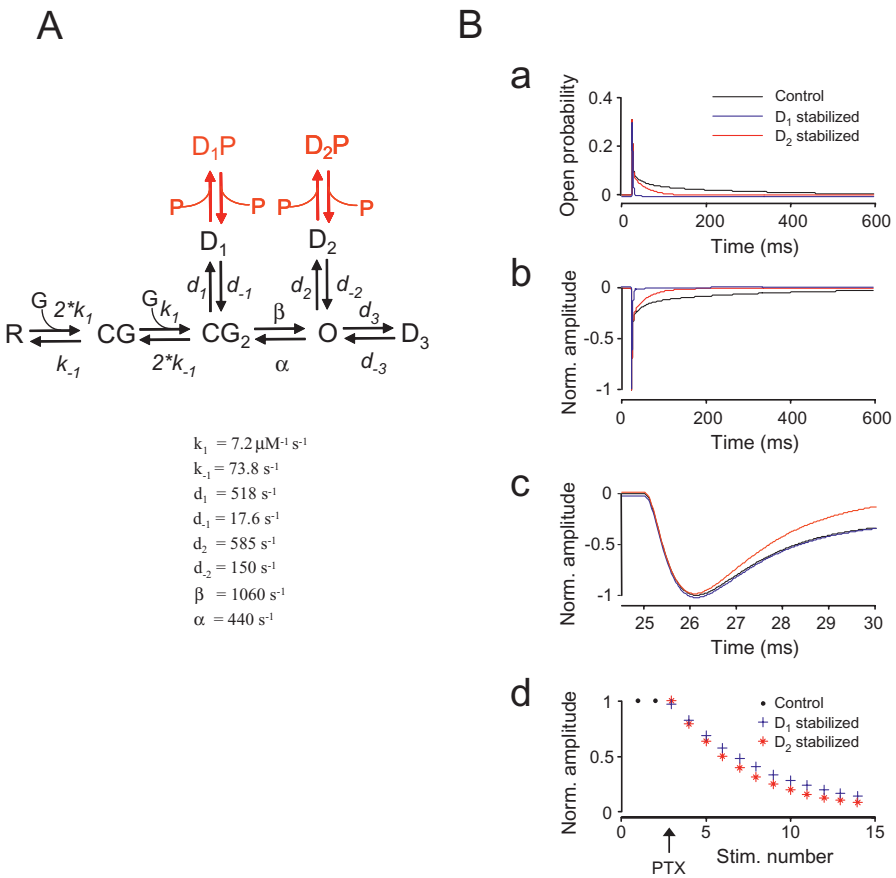

Figure 8 Simulation of the interaction of PTX with the $GABA_A$ receptor based on the kinetic scheme proposed by Burkat *et al.* (2001). (A) Kinetic scheme showing transitions presented by Burkat *et al.* (2001) for the native $GABA_A$ receptor and the microscopic rate constants for expressed $\alpha_1\beta_1\gamma_2$ receptors below. R, represents the unbound, non-conducting receptor, CG, is a singly bound closed state. Binding of a second molecule of GABA promotes entry into the closed state, CG_2. D_1 is a fast desensitizing state entered from CG_2. O is the open state also entered from CG_2. O can enter two desensitized states: D_2, which is entered rapidly, and D_3, which is entered slowly and is extremely stable (implying that further stabilization of D_3 by PTX would be of no significant consequence). We therefore focused on the desensitized states, D_1 and D_2, as likely targets for interaction with PTX (P) and have appended the bound complexes, D_1P and D_2P. (B) Stabilization of the desensitized states, D_1 and D_2. Details of the panels are as described in the legend to Figure 7. Stabilization of either D_1 or D_2 results in accelerated decay (B,b,c), without affecting the rise-time of normalized responses (B,c). Stabilization of either state gives a gradual reduction in amplitude on repeated stimulation and the initial peak open probability was virtually unaffected (B,d). The acceleration of D_2-stabilized responses was greater and initiated earlier than D_1-stabilized responses. Thus, although stabilization of D_2 displays the qualitatively closest agreement with the experimental findings, both mechanisms must be considered likely (see Discussion).

of current can occur. Therefore, a finite decay rate will only be observed if there is at least one open state that is not occluded by PTX and that is accessible through path(s) that circumvent(s) PTX-occludable open states. In other words, PTX cannot block all open states of the $GABA_A$ receptor by means of open-channel mechanisms. Thus, the gating scheme for an open-channel block must include at least two open states, of which one is occluded by PTX and one is not. Note that this restriction does not exclude the possibility of allosteric inhibition of open states that are not occluded by PTX. That is to say an open-channel block and allosteric modulation may coexist. Thus, the above constraint invalidates transition schemes with only one open state, such as that proposed by Burkat *et al.* (2001) (Figure 8A). A simple and commonly used transition scheme has been proposed by Jones and Westbrook (1995) (Figure 7A). This contains two open states and does not, therefore, violate the above constraint. We simulated the situation in which each of the open states (O_1 and O_2) in turn is susceptible to pore occlusion by PTX. Occlusion of O_1 by PTX yields a response that is virtually identical to the simulated control eIPSC (Figure 7Bb,c), which is not in accordance with the observed acceleration of experimental eIPSCs (Figure 2). On the other hand, occlusion of O_2 causes an immediate and complete reduction of peak open probability (Figure 7Ba), with a corresponding abrupt reduction of single responses following PTX (Figure 7Bd). Furthermore, occlusion of O_2 reduces the rise time of the normalized response (Figure 7Bc). Occlusion of O_1 or O_2 is not, therefore, in accordance with our experimental observations (Figures 1 and 2, respectively) and must be considered extremely unlikely.

The case for allosteric modulation by PTX

In the case of allosteric modulation, it is assumed that PTX either stabilizes non-conducting states or destabilizes conducting states. Stabilization of non-conducting states has previously found compelling support in studies on macroscopic currents evoked by ultrarapid application techniques

(Ramakrishnan and Hess, 2005), as well as the aforementioned single-channel studies. In the latter, the action of PTX was accompanied by reductions both in general and intra-burst opening frequency, as well as burst duration and frequency (Twyman *et al.*, 1989; Newland and Cull-Candy, 1992; Ikeda *et al.*, 1998), along with increased shut times (Ikeda *et al.*, 1998) and frequency of long shut periods (Newland and Cull-Candy, 1992).

With allosteric modulation, the observation of a finite decay rate only allows us to impose the following relatively liberal constraint on the kinetic scheme. There must be a traversable path(s) leading from the GABA unbound receptor state into an open state, whether PTX is bound or not. Schemes that violate this constraint will completely abolish entry into open states. For example, the restriction invalidates direct stabilization of $Bound_1$ in Figure 7A and CG_1 and CG_2 in Figure 8A. Most proposed kinetic schemes of $GABA_A$ receptor transition include non-conducting states that may serve as targets for stabilization by PTX. For example, the model proposed by Jones and Westbrook (1995) includes two desensitized states (D_1 and D_2) as well as one GABA-bound, non-conducting state ($Bound_2$) (Figure 7A), all of which obey the above constraint. Stabilization of D_1 results in a response that is identical to the control (Figure 7Ca–c), while stabilization of $Bound_2$ immediately and markedly reduces peak open probability (Figure 7Ca) and furthermore reduces the rise time of the response (Figure 7Cc). None of these predictions are in accordance with the experimental observations (Figure 2) and must therefore be considered extremely unlikely. On the other hand, stabilization of D_2 produces a response that is qualitatively similar to the experimental eIPSCs in the presence of PTX (compare Figures 2 with 7Cb,c). The peak open probability is unaltered on the first response after exposure to PTX (Figures 1 and 7Ca,d). Thereafter, the peak open probability declines gradually in parallel with the amplitude (Figures 1 and 7Cd). The rise time of the normalized response is unaffected (Figures 2 and 7Cc), while the decay phase is accelerated (Figures 2 and 7Cb). Furthermore, the accelerated decay showed a monoexponential time course. The slow component (τ_{slow}) had been completely eliminated, while τ_{fast} increased by 17.7% (from 200 to 242 ms). While the latter result is not in complete agreement with the experimental observations (Figure 5), stabilization of D_2 remains a very likely mechanism of PTX inhibition in the model proposed by Jones and Westbrook (1995).

In order to test for the possibility that PTX stabilizes desensitized states that are in series with an open state, simulations were made by using the transition scheme of Burkat *et al.* (2001) (see Figure 8A and Methods). Because the observed kinetics are significantly altered in the experimental setting (Figure 2), the very long-lived desensitized state, D_3, was not included in the simulation. Stabilization of D_1 as well as D_2 resulted in many qualitative similarities with the eIPSCs of cultured neurones: rise times and peak open probabilities are unaffected by PTX (Figure 8Ba,c), while the decay phases are significantly accelerated (Figure 8Bb). Stabilization of D_1 resulted in a reduction of τ_{fast} by 35.5% (from 26.3 to 17.5 ms) and τ_{slow} by 84.8% (from 2246 to 343 ms), while the relative amplitude of the fast component was decreased by 6.8% (from 82.7 to 75.9%), and that of the slow component correspondingly increased. Thus, stabilization of D_1 was in overall agreement with the experimentally observed responses.

Stabilization of D_2 resulted in a monoexponential decay with a time constant of 20.2 ms. This represents a reduction of τ_{fast} by 23% (from the control value of 26.3 ms) and a complete abolishment of the slow component. These findings are in very close agreement with the experimental observations and suggest that stabilization of D_2 is a very likely target for the action of PTX. Furthermore, in the case of stabilization of D_2, the increase in rate of decay started just after the peak (Figure 8Bc), as was observed for experimental eIPSCs in the presence of PTX (Figure 2C,D). This contrasts with the later acceleration with stabilization of D_1 (Figure 8Bb,c). Thus, while stabilization of D_1 cannot be excluded, stabilization of D_2 yields a qualitatively better agreement with the experimental results. Therefore, we propose that this constitutes the main mechanism of inhibition by PTX.

The open-channel block and allosteric mechanisms discussed above have one common feature: inhibition is obtained by the addition of a single non-conducting state in series with the state under investigation (Figures 7A and 8A). However, alteration of existing rate constants is also a possibility. Destabilization of open states, which finds support in the previously observed reduction of the intraburst open duration (Twyman *et al.*, 1989 – see above), serves as a relevant example of such alterations. The relationship between alterations of existing rate constants and the shape of macroscopic currents has been investigated thoroughly by Bianchi *et al.* (2007). However, information about the degree of 'coupling' (correlation) between deactivation and desensitization of the currents is a prerequisite for their algorithmic approach and cannot, therefore, be applied to our present results of macroscopic recordings of eIPSCs (see Future Perspectives).

Although geometric considerations led Erkkila *et al.* (2008) to conclude that a non-competitive pore blocking mechanism must be involved with the action of PTX (*vide supra*), these findings can also be incorporated with the proposal that PTX is an allosteric modulator that stabilizes desensitized state(s). The PTX binding site is known to be deep within the pore (Olsen, 2006; Erkkila *et al.*, 2008), which would have to be open for the sizeable PTX molecule to gain access. The desensitized state(s) involve conformational change(s) such that the channel cannot conduct Cl^- ions. It might be surmised that the three polar groups identified by Erkkila *et al.* (2008) become aligned such that they readily engage with PTX. With a low dissociation constant, the complex is essentially locked in this state. It is, however, a moot point as to whether PTX is an open-channel blocker, for the channel must be open for PTX to reach its binding site. Whether the complex has to be desensitized in order for PTX to bind or its binding actually induces desensitization is not presently resolved.

In summary, analysis of simulated responses allows us to exclude the possibility of an open-channel block as the mechanism of antagonism by PTX. The results indicate that PTX probably stabilizes desensitized states such as D_2 in the transition scheme proposed by Jones and Westbrook (1995) and/or D_2 (and possibly D_1) in the model proposed by Burkat *et al.* (2001). The effect of increasing PTX concentration

would be expected to reduce resensitization to such an extent that the receptor is effectively trapped in the desensitized state.

Future perspectives

It would be relevant to study the time-dependent component of PTX-induced inhibition in isolation. This might be found to involve a completely different mechanism and/or binding site(s) from that involved in the use-dependent block presented here.

Finally, it would be interesting to investigate the degree of coupling between macroscopic desensitization and deactivation in an outside-out patch configuration using specifically expressed receptor systems and rapid application. This would allow us to address whether PTX alters existing transition rate constants of a given model using the relatively simple algorithmic considerations presented by Bianchi *et al.* (2007).

Conclusions and implications

The present study represents the first thorough investigation of the action of PTX on naturally evoked GABA receptor-mediated IPSCs. Both the results and simulations indicate that the use-dependent aspect of inhibition by PTX is unlikely to be mediated by direct pore occlusion, but rather by stabilization of GABA bound desensitized state(s) of the $GABA_A$ receptor.

Acknowledgements

The expert technical assistance of Sys Kristiansen, Brita Holst Jensen and Puk Lund is gratefully acknowledged. All authors are supported by the Danish Medical Research Council. JDCL received support for Aarhus University Research Foundation and KJ from Gangsted Foundation (DK), Lægeforeningens Forskningsfond (DK), Foundation for Research in Neurology (DK), Lundbeck Foundation (DK).

Conflict of Interests

None.

References

Alexander SPH, Mathie A, Peters JA (2008). Guide to receptors and channels (GRAC). *Br J Pharmacol* **153** (Suppl. 2): S1–S209.

Bianchi MT, Botzolakis EJ, Haas KF, Fisher JL, Macdonald RL (2007). Microscopic kinetic determinants of macroscopic currents: insights from coupling and uncoupling of $GABA_A$ receptor desensitization and deactivation. *J Physiol* **584**: 769–787.

Burkat PM, Yang J, Gingrich KJ (2001). Dominant gating governing transient $GABA_A$ receptor activity: a first latency and $P_{o/o}$ analysis. *J Neurosci* **21**: 7026–7036.

Chen L, Durkin KA, Casida JE (2006). Structural model for γ-aminobutyric acid receptor noncompetitive antagonist binding: widely diverse structures fit the same site. *Proc Natl Acad Sci USA* **103**: 5185–5190.

Colquhoun D, Hawkes AG (1995). The principles of the stochastic interpretation of ion-channel mechanisms. In: Sakmann B, Neher E (eds). *Single Channel Recording*, 2nd edition. Plenum Press: New York: 397–479.

Curtis DR, Johnston GAR (1974). Amino acid transmitters in the mammalian central nervous system. *Ergebn Physiol* **69**: 97–188.

Curtis DR, Duggan AW, Johnston GAR (1969). Glycine, strychnine, picrotoxin and spinal inhibition. *Brain Res* **14**: 759–762.

Dillon GH, Im WB, Carter DB, McKinley DD (1995). Enhancement by GABA of the association rate of picrotoxin and *tert*-butylbicyclophosphorothionate to the rat cloned $\alpha1\beta2\gamma2$ $GABA_A$ receptor subtype. *Br J Pharmacol* **115**: 539–545.

Drasbek KR, Jensen K (2006). THIP, a hypnotic and antinociceptive drug, enhances an extrasynaptic $GABA_A$ receptor-mediated conductance in mouse neocortex. *Cereb Cortex* **16**: 1134–1141.

Erkkila BE, Weiss DS, Wotring VE (2004). Picrotoxin-mediated antagonism of α_3 β_4 and α_7 acetylcholine receptors. *NeuroReport* **15**: 1969–1973.

Erkkila BE, Sedelnikova AV, Weiss DS (2008). Stoichiometric pore mutations of the $GABA_AR$ reveal a pattern of hydrogen bonding with picrotoxin. *Biophys J* **94**: 4299–4306.

Halm DR (1998). Identifying swelling-activated channels from ion selectivity patterns. *J Gen Physiol* **112**: 369–371.

Holm MM, Korshoej AR, Lambert JDC, Jensen K (2007). Single axon fiber stimulation in rat hippocampus: effects of the plant convulsant, picrotoxin, on IPSC amplitude and decay kinetics. *Soc Neurosci Abstr* **33**: 142.25.

Ikeda T, Nagata K, Shono T, Narahashi T (1998). Dieldrin and picrotoxinin modulation of GABA(A) receptor single channels. *NeuroReport* **9**: 3189–3195.

Inoue M, Akaike N (1988). Blockade of γ-aminobutyric acid-gated chloride current in frog sensory neurons by picrotoxin. *Neurosci Res* **5**: 380–394.

Jensen K, Jensen MS, Lambert JDC (1999a). Post-tetanic potentiation of GABAergic IPSCs in cultured rat hippocampal neurones. *J Physiol* **519**: 71–84.

Jensen K, Lambert JDC, Jensen MS (1999b). Activity-dependent depression of GABAergic IPSCs in cultured hippocampal neurons. *J Neurophysiol* **82**: 42–49.

Jones MV, Westbrook GL (1995). Desensitized states prolong $GABA_A$ channel responses to brief agonist pulses. *Neuron* **15**: 181–191.

Korshoej AR, Lambert JDC (2007). Post-tetanic potentiation of GABAergic IPSCs in cultured hippocampal neurones is exclusively time-dependent. *Brain Res* **1138**: 39–47.

Korshoej AR, Holm MM, Jensen K, Lambert JDC (2007). Blockade of GABAergic IPSCs in cultured hippocampal neurones by picrotoxin: kinetic analysis provides insight into mechanism. *Soc Neurosci Abstr* **33**: 142.24.

Krishek BJ, Moss SJ, Smart TG (1996). A functional comparison of the antagonists bicuculline and picrotoxin at recombinant $GABA_A$ receptors. *Neuropharmacology* **35**: 1289–1298.

Lambert JDC, Korshoej AR (2008). Picrotoxin blocks IPSCs on cultured hippocampal neurones by stabilizing desensitized state(s) of the $GABA_A$ receptor. *FENS Abstr* **4**: 11.14.

Li P, Slaughter M (2007). Glycine receptor subunit composition alters the action of GABA antagonists. *Vis Neurosci* **24**: 513–521.

Mangan PS, Sun C, Carpenter M, Goodkin HP, Sieghart W, Kapur J (2005). Cultured hippocampal pyramidal neurons express two kinds of $GABA_A$ receptors. *Mol Pharmacol* **67**: 775–788.

Moffatt L (2007). Estimation of ion channel kinetics from fluctuations of macroscopic currents. *Biophys J* **93**: 74–91.

Newland CF, Cull-Candy SG (1992). On the mechanism of action of picrotoxin on GABA receptor channels in dissociated sympathetic neurones of the rat. *J Physiol* **447**: 191–213.

Olsen RW (2006). Picrotoxin-like channel blockers of $GABA_A$ receptors. *Proc Natl Acad Sci USA* **103**: 6081–6082.

Porter NM, Angelotti TP, Twyman RE, Macdonald RL (1992). Kinetic properties of $\alpha_1\beta_1$ γ-aminobutyric $acid_A$ receptor channels expressed

in Chinese hamster ovary cells: regulation by pentobarbital and picrotoxin. *Mol Pharmacol* **42**: 872–881.

Ramakrishnan L, Hess GP (2005). Picrotoxin inhibition mechanism of a γ-aminobutyric acid$_A$ receptor investigated by a laser-pulse photolysis technique. *Biochemistry* **44**: 8523–8532.

Sedelnikova A, Erkkila BE, Harris H, Zakharkin SO, Weiss DS (2006). Stoichiometry of a pore mutation that abolishes picrotoxin-mediated antagonism of the GABA$_A$ receptor. *J Physiol* **577**: 569–577.

Smart TG, Constanti A (1986). Studies on the mechanism of action of picrotoxinin and other convulsants at the crustacean muscle GABA receptor. *Proc R Soc Lond B* **227**: 191–216.

Takeuchi A, Takeuchi N (1969). A study of the action of picrotoxin on the inhibitory neuromuscular junction of the crayfish. *J Physiol* **205**: 377–391.

Twyman RE, Rogers CJ, Macdonald RL (1989). Pentobarbital and picrotoxin have reciprocal actions on single GABA$_A$ receptor channels. *Neurosci Lett* **96**: 89–95.

Wang DS, Buckinx R, Lecorronc H, Mangin JM, Rigo JM, Legendre P (2007). Mechanisms for picrotoxinin and picrotin blocks of α_2 homomeric glycine receptors. *J Biol Chem* **282**: 16016–16035.

Yoon K-W, Covey DF, Rothman SM (1993). Multiple mechanisms of picrotoxin block of GABA-induced currents in rat hippocampal neurons. *J Physiol* **464**: 423–439.